Asian Journal of Chemistry; Vol. 37, No. 10 (2025), 2605-2611
ASIAN JOURNAL OF CHEMISTRY
https://doi.org/10.14233/ajchem.2025.34552

Hydrothermal Synthesis of Z-Scheme $ZnWO_4$/BiOBr Nanocomposite for Photocatalytic Degradation of Rhodamine B Dye

MOHAMMAD FARHAN[1], ANIL KUMAR SINGH[1] and GANDHARVE KUMAR[2,*]

[1]Department of Chemistry, Faculty of Engineering, Teerthanker Mahaveer University, Moradabad-244001, India
[2]Department of Chemistry, School of Basic Sciences, Galgotias University, Greater Noida-203201, India

*Corresponding author: E-mail: gandharve.kumar@galgotiasuniversity.edu.in

Received: 28 July 2025 *Accepted*: 25 September 2025 *Published online*: 30 September 2025 AJC-22146

The $ZnWO_4$/BiOBr heterostructured photocatalyst was prepared using a hydrothermal synthesis method and systematically characterized using advanced analytical techniques. Its photocatalytic performance was evaluated under simulated sunlight, demonstrating efficient degradation of rhodamine B (RhB) dye. The best performing 10 wt.% $ZnWO_4$/BiOBr photocatalysts remove about 99% RhB (10 mg/L), whose photocatalytic degradation rate was 17-times and 5-times superior than $ZnWO_4$ and BiOBr parent materials, respectively. The enhanced photocatalytic efficiency of the 10 wt.% $ZnWO_4$/BiOBr nanocomposite under visible light is attributed to its favourable band alignment resembling a Z-scheme mechanism, which facilitates effective charge separation, suppresses electron-hole recombination and promotes the *in situ* generation of reactive oxygen species.

Keywords: Z-scheme, $ZnWO_4$, BiOBr, Solar photocatalyst, Dye degradation.

INTRODUCTION

The acceleration of industrialization across the globe has intensified environmental challenges with water contamination and energy shortages emerging as critical concerns. Among various forms of aquatic pollution, the discharge of residual effluents from textile manufacturing has garnered substantial attention due to its ecological and public health implications [1,2]. Cationic dyes, particularly rhodamine B, are widely employed in textile and related industries because of their vibrant colour properties and stability [3-5]. However, their strong affinity for water and resistance to degradation make them persistent pollutants, posing significant risks to aquatic ecosystems and human health [6,7]. To mitigate the environmental burden of these dyes, various treatment technologies have been investigated, among which semiconductor-based heterogeneous photocatalysis has emerged as a promising strategy for degrading organic pollutants in wastewater. Despite their potential, conventional semiconductor photocatalysts are often limited by poor redox activity, structural defects and high recombination rates of photoinduced electron-hole pairs, which restrict their photocatalytic efficiency [8-10]. Consequently, there is a compelling need for the development of robust, stable and sunlight-responsive photocatalysts capable of efficiently degrading dyes under solar irradiation. In recent years, bismuth based photocatalysts have attracted considerable interest owing to their unique layered structures and excellent visible-light responsiveness [11]. Photocatalysts such as Bi_2WO_6 [12], $BiVO_4$ [13], Bi_2MoO_6 [14] and Bi_2S_3 [15] have been extensively studied due to the favourable electronic configuration of Bi^{3+} ions ($6s^2$). Among these, bismuth oxybromide (BiOBr) stands out as a promising material due to its layered tetragonal structure, environmental benignity, non-toxicity and superior chemical stability [16].

However, pristine BiOBr exhibits a wide band gap, leading to rapid recombination of photogenerated charge carriers and limited photocatalytic activity. To address this issue, the construction of heterojunction systems, especially Z-scheme nanocomposites, has been widely explored [17]. Such systems involve the integration of BiOBr with semiconductors possessing appropriately aligned band edge positions [18,19]. The Z-scheme heterostructure offers significant advantages by promoting efficient charge separation while preserving strong redox potentials. In this configuration, photogenerated electrons and holes are spatially confined within different semiconductors, which promotes the formation of reactive oxygen species essential for photocatalytic reactions [20-22].

Several studies have demonstrated the superior photocatalytic performance of BiOBr-based heterojunctions. Qiu *et al.* [23] reported a SnS_2/BiOBr composite exhibiting significant enhancement in rhodamine B dye degradation. Similarly, Hu *et al.* [24] synthesized a Sn_3O_4/BiOBr type-II heterojunction, which displayed remarkable activity in dye removal. Furthermore, Raizada *et al.* [25] developed a novel Ag-AgCl/BiOBr Z-scheme photocatalyst that effectively eliminated phenol from aqueous media. These advances underscore the potential of BiOBr-based heterostructures in the sustainable treatment of dye-contaminated wastewater. The photocatalytic performance of BiOBr can be significantly improved by incorporating $ZnWO_4$ as a sensitizer, owing to the well-matched band edge positions of $ZnWO_4$ and BiOBr.

In this study, a novel $ZnWO_4$/BiOBr heterostructure was synthesized through a two-step hydrothermal method and thoroughly characterized to evaluate its morphological, structural and optical properties. The results suggest the successful formation of a well-coupled nanocomposite, with evidence supporting the establishment of a Z-scheme heterojunction between $ZnWO_4$ and BiOBr, promising for enhanced photocatalytic performance.

EXPERIMENTAL

Zinc nitrate hexahydrate, sodium tungstate, potassium bromide, isopropyl alcohol chloroform and ammonium oxalate, rhodamine B dye were procured from Rankem Pvt. Ltd., India. The crystalline phases were analyzed using a Bruker AXS diffractometer with a graphite-monochromated Cu*K*α radiation source (λ = 1.5418 Å), operated at 40 kV and a scan rate of 1º min^{-1}. Surface morphology was investigated using field-emission scanning electron microscopy (FE-SEM, Zeiss Ultra Plus 55) at an accelerating voltage of 20 kV. Optical absorption spectra were recorded using a Shimadzu UV-2450 spectrophotometer (Japan) with $BaSO_4$ employed as reference material.

Synthesis of $ZnWO_4$ nanoparticles: Firstly, $ZnWO_4$ nanoparticles were prepared by the hydrothermal method. Mixture A containing $Zn(NO_3)_2{\cdot}6H_2O$ (1.4874 g) in 25 mL of deionized water was added to a mixture B comprising of 1.649 g $Na_2WO_4{\cdot}2H_2O$ in 25 mL deionized water and continuously stirred for 0.5 h. The final suspension was put into autoclave and placed at 200 ºC in oven for 12 h. Finally, the supernatant liquid was disposed of and the final product was gathered, cleaned with water and ethanol and then let too dry at 50 ºC.

Synthesis of $ZnWO_4$/BiOBr photocatalyst: Initially, KBr (2 mmol) and bismuth nitrate pentahydrate (2 mmol) was mixed in 50 mL of deionized water and the final solution was continuously stirred for 0.5 h. The pH of the solution was adjusted at 6 using a 10 M NaOH solution. Subsequently, specific amounts of $ZnWO_4$ (5, 10 and 15 wt.%) were added to the mixture, which was then stirred continuously for 1.5 h. The resulting suspension was transferred into a 100 mL Teflon-lined autoclave and subjected to hydrothermal treatment at 100 ºC for 12 h. After the reaction, the synthesized $ZnWO_4$/BiOBr photocatalyst samples were collected, washed thoroughly, and dried at 60 ºC overnight.

RESULTS AND DISCUSSION

XRD studies: The crystalline structure of 10 wt.% $ZnWO_4$/BiOBr composite, along with its individual components (pure $ZnWO_4$ and BiOBr), was examined using X-ray diffraction (XRD) and the corresponding patterns are displayed in Fig. 1. The diffraction peaks of pure BiOBr and $ZnWO_4$ matched well with the tetragonal phase of BiOBr (JCPDS No. 85-681) and the mono clinic scheelite-type phase of $ZnWO_4$ (JCPDS No. 14-0688), respectively [23,26]. Notably, the XRD pattern of the 10 wt.% $ZnWO_4$/BiOBr composite clearly exhibited the characteristic diffraction peaks corresponding to $ZnWO_4$, confirming its successful incorporation into the heterostructure.

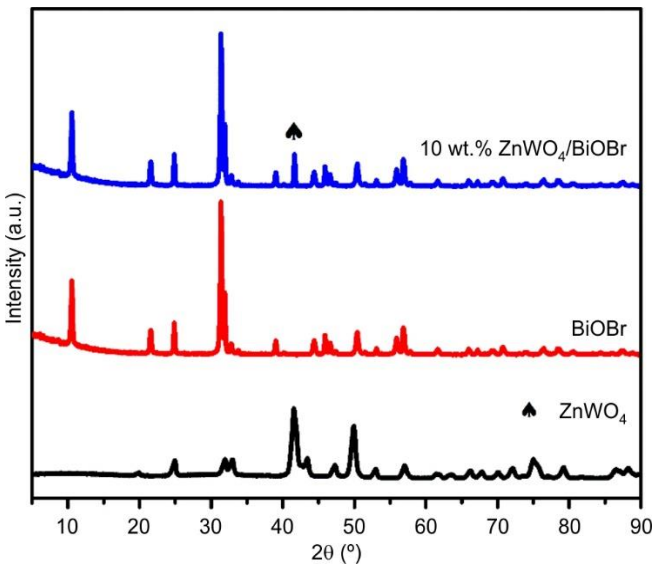

Fig. 1. XRD patterns of BiOBr, $ZnWO_4$ and 10 wt.% $ZnWO_4$/BiOBr nanocomposite

Morphological studies: The surface morphology and particle size of the as-prepared pure $ZnWO_4$, BiOBr and their 10 wt.% composite ($ZnWO_4$/BiOBr) were investigated through scanning electron microscopy (SEM). As shown in Fig. 2a, the $ZnWO_4$ sample consisted of nanoparticles with irregular shapes, with diameters ranging from approximately 70 to 90 nm. In contrast, the SEM image of pure BiOBr (Fig. 2b) displayed plate-like structures with non-uniform morphology and lateral sizes between 300 and 600 nm. The FESEM image of 10 wt.% $ZnWO_4$/BiOBr composite (Fig. 2c) revealed that $ZnWO_4$ nanoparticles were uniformly anchored onto the surface of the BiOBr nanoplates, indicating good interfacial contact between the two components.

Optical properties and band structure analysis: The optical band gaps of pure $ZnWO_4$, BiOBr and 10 wt.% $ZnWO_4$/BiOBr composite were evaluated using UV-vis DRS method. The corresponding Tauc plots, derived from the $(\alpha h\nu)^2$ *vs.* hν relationship, are shown in Fig. 3. The estimated band gap energies (E_g) were found to be approximately 3.50 eV for $ZnWO_4$, 2.86 eV for BiOBr and 2.92 eV for 10 wt.% $ZnWO_4$/BiOBr heterojunction.

To further understand the band structure, the conduction band (E_{CB}) and valence band (E_{VB}) edge potentials were calculated using the following equations.

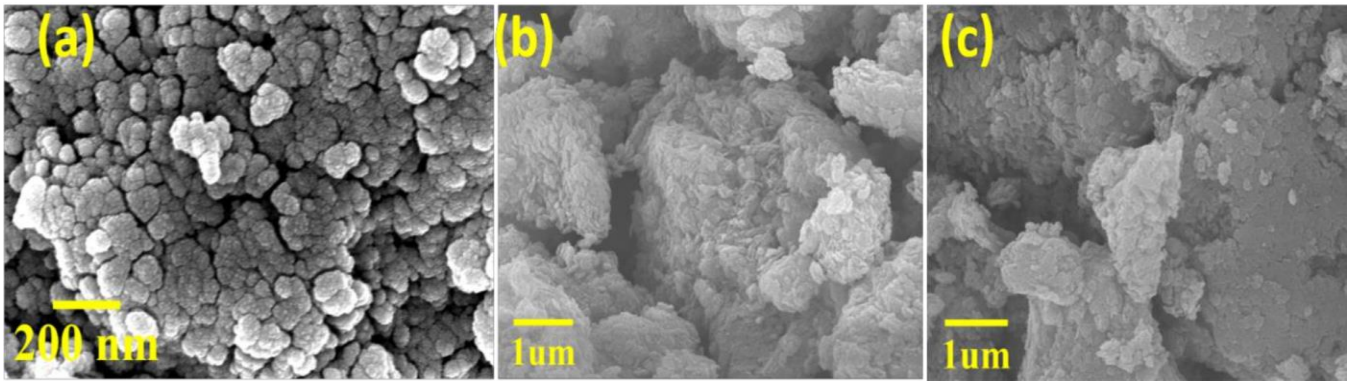

Fig. 2. SEM image of (a) $ZnWO_4$; (b) BiOBr; (c) 10 wt.% $ZnWO_4$/BiOBr

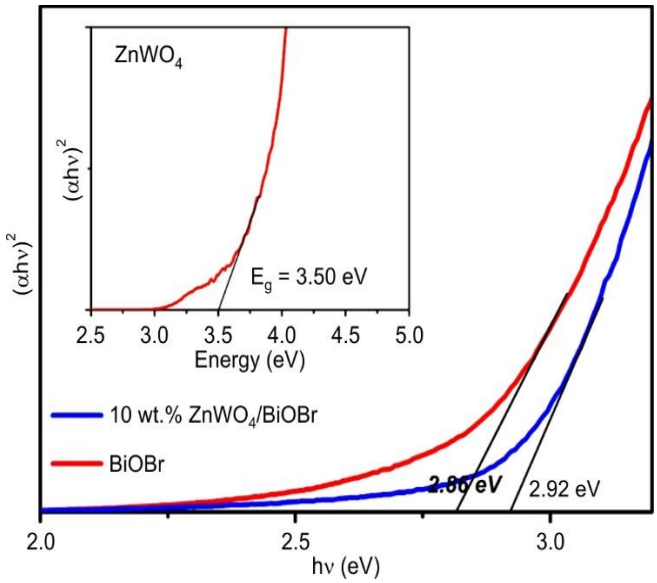

Fig. 3. The relative band gap energy of $ZnWO_4$ (inset), BiOBr and 10 wt.% $ZnWO_4$/BiOBr

$$E_{VB} = \chi - E_e + \frac{1}{2}E_g \text{ and } E_{CB} = E_{VB} - E_g$$

The E_{CB} and E_{VB} represent conduction band and valence band energies, respectively, E_g represents band gap energy, χ values for $ZnWO_4$ and BiOBr is 5.44 eV and 6.18 eV for respec-tively and E_e (energy of free electron). The E_{CB} and E_{VB} values of BiOBr are 0.22 eV and 3.14 eV. Similarly, the value of conduction band (E_{CB}) and valence band (E_{VB}) of $ZnWO_4$ are -1.31 and 2.19 eV, respectively.

Photocatalyst studies: The UV-visible absorption spectra of rhodamine B (RhB) solution (10 mg/L) treated with a photocatalyst dose of 0.6 mg/mL are shown in Fig. 4a. Prior to light irradiation, the adsorption-desorption equilibrium was established in the dark. Subsequently, the samples were exposed to the natural sunlight. The time-dependent decrease in the normalized concentration of RhB (C_t/C_o) during irradiation is shown in Fig. 4b. The degradation behaviour followed a pseudo-first-order kinetic model, as evidenced by the linear fit in Fig. 4c. Control experiments without a photocatalyst confirmed that photolysis of RhB under identical conditions was negligible (Fig. 4b, Table-1).

TABLE-1
ADSORPTION AND DEGRADATION EXPERIMENTS SUMMARY

Photocatalysts	Ads. (%)	Deg. (%)	Rate constant (min^{-1})
15 wt.% $ZnWO_4$/BiOBr	21%	82%	0.020
10 wt.% $ZnWO_4$/BiOBr	23%	99%	0.035
5 wt.% $ZnWO_4$/BiOBr	20%	74%	0.015
BiOBr	12%	42%	0.007
$ZnWO_4$	20%	37%	0.002
Blank	NA	10%	0.001

The influence of photocatalyst dosage and initial RhB concentration on degradation efficiency was also investigated. The comparative photocatalytic tests were conducted using pure $ZnWO_4$, pristine BiOBr and $ZnWO_4$/BiOBr composites with varying $ZnWO_4$ loadings. The results are summarized in Fig. 5. The corresponding degradation efficiencies and rate constants are presented in Table-1. Among the tested materials, 10 wt.% $ZnWO_4$/BiOBr nanocomposite demonstrated superior photocatalytic activity, achieving ~99% RhB degradation within 80 min of sunlight exposure. This performance was nearly five times higher than that of pristine BiOBr.

The enhanced activity of 10 wt.% $ZnWO_4$/BiOBr composite is attributed to the effective formation of a heterojunction, which promotes efficient charge carrier separation and minimizes electron–hole recombination. In contrast, 5 wt.% composite exhibited relatively poor performance, likely due to insufficient $ZnWO_4$ content, limiting light absorption and charge separation efficiency. The 15 wt.% composite also exhibited the reduced activity, possibly due to the excess $ZnWO_4$ obstructing active sites on the BiOBr surface. The apparent rate constant (k) for RhB degradation using 10 wt.% $ZnWO_4$/BiOBr catalyst was found to be 0.035 min^{-1}, significantly higher than those for pure BiOBr (0.007 min^{-1}) and $ZnWO_4$ (0.002 min^{-1}), under the similar conditions. The improved photocatalytic efficiency of the $ZnWO_4$/BiOBr composites is due to the enhanced charge carrier dynamics and the generation of reactive oxygen species (ROS).

Mechanistic insight *via* scavenger studies: To further elucidate the photocatalytic mechanism, ROS scavenging experiments were conducted using 10 wt.% $ZnWO_4$/BiOBr catalyst in the presence of various scavengers. Isopropyl alcohol

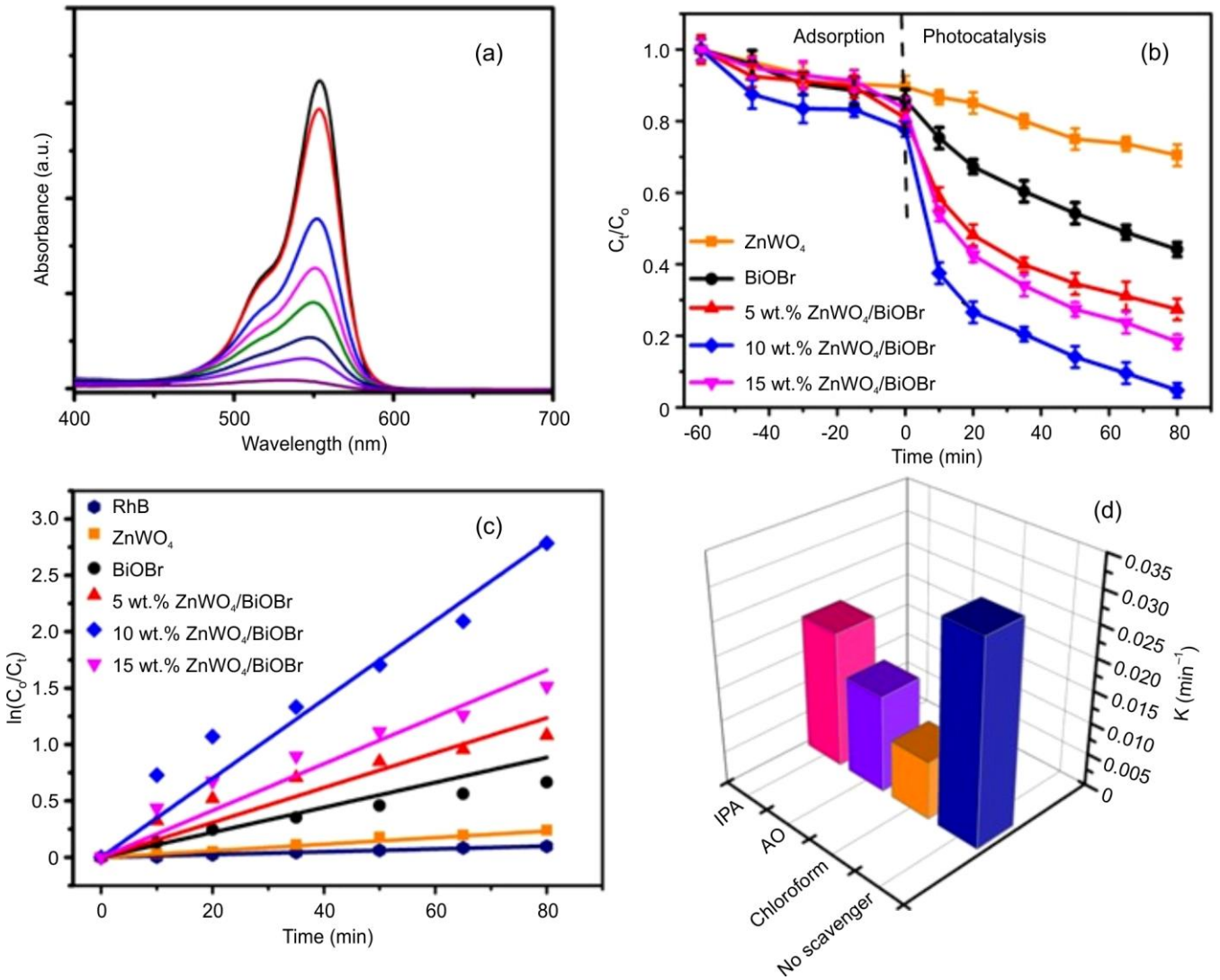

Fig. 4. (a) Absorption spectrum of RhB degradation, (b-c) degradation and pseudo-first-order kinetic plot RhB by $ZnWO_4$, BiOBr and $ZnWO_4$/BiOBr nanocomposites and (d) scavenger studies

(IPA), ammonium oxalate (AO) and chloroform were employed to quench hydroxyl radicals (•OH), photogenerated holes (h^+) and superoxide radicals ($O_2^{-\bullet}$), respectively [27]. The results (Fig. 4d) revealed a significant reduction in RhB degradation efficiency upon addition of scavengers, indicating the active involvement of these species in the degradation process. Among them, chloroform exhibited the strongest inhibitory effect, highlighting the crucial role of superoxide radicals. A noticeable decline in efficiency was also observed with AO, confirming the contribution of photogenerated holes to the degradation mechanism.

Reusability: The recyclability of 10 wt.% $ZnWO_4$/BiOBr photocatalyst was assessed over five consecutive cycles of RhB degradation under sunlight. The catalyst retained its photocatalytic activity with the minimal loss in performance, demonstrating its excellent stability (Fig. 6a). The post-reaction structural analysis using powder X-ray diffraction (pXRD) revealed no significant changes in the crystalline structure after repeated use (Fig. 6b), confirming the structural integrity and durability of the composite photocatalyst.

Photocatalytic mechanism: The efficiency of charge carrier separation and transfer in heterojunction-based photocatalysts is highly dependent on the appropriate alignment of the band edge positions of the constituent semiconductors. In case of the $ZnWO_4$/BiOBr heterostructure, the conduction band (E_{CB}) of $ZnWO_4$ possesses a more negative potential compared to that of BiOBr. Consequently, in a conventional type-II heterojunction configuration, photogenerated electrons would transfer from the E_{CB} of $ZnWO_4$ to the valence band (E_{VB}) of BiOBr, where they would recombine with holes. However, the E_{CB} potential of BiOBr is more positive than the reduction potential required to convert molecular oxygen (O_2) to superoxide radical anion ($O_2^{-\bullet}$), which is approximately -0.33 eV [28]. As a result, under a type-II mechanism, it would be energetically unfavourable for electrons in BiOBr conduction band to reduce O_2 into $O_2^{-\bullet}$. This contradicts the results of radical scavenging experiments, which indicated that $O_2^{-\bullet}$ plays a pivotal role in the degradation of RhB molecules (Fig. 7). To reconcile these findings, an alternative Z-scheme mechanism is also proposed for the photocatalytic activity of the $ZnWO_4$/BiOBr

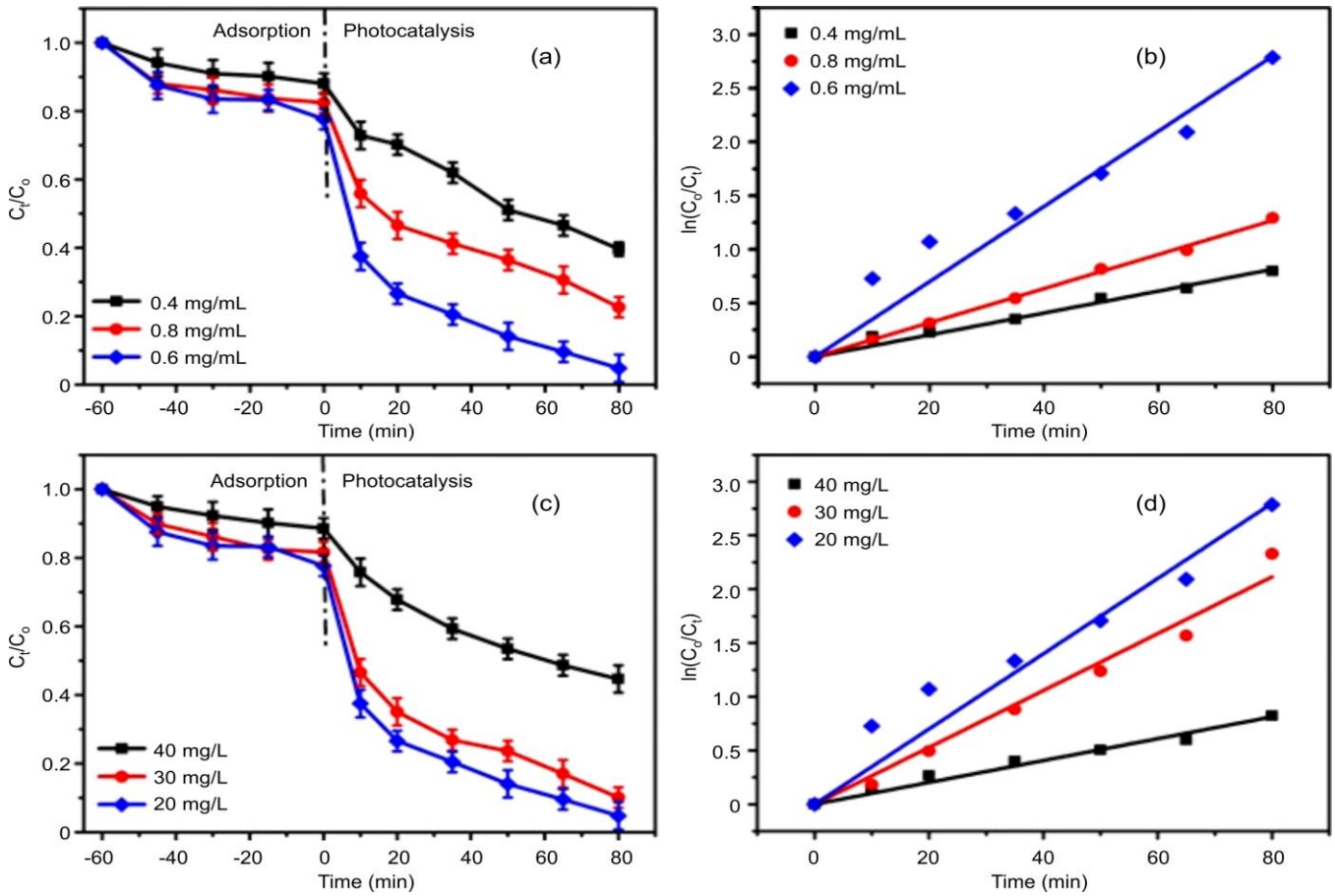

Fig. 5. (a) Photocatalyst dose influence on the photocatalytic efficiency (b) I[st]-order kinetics studies, (c) RhB concentration influence on photocatalyst activity, (d) I[st]-order kinetics studies

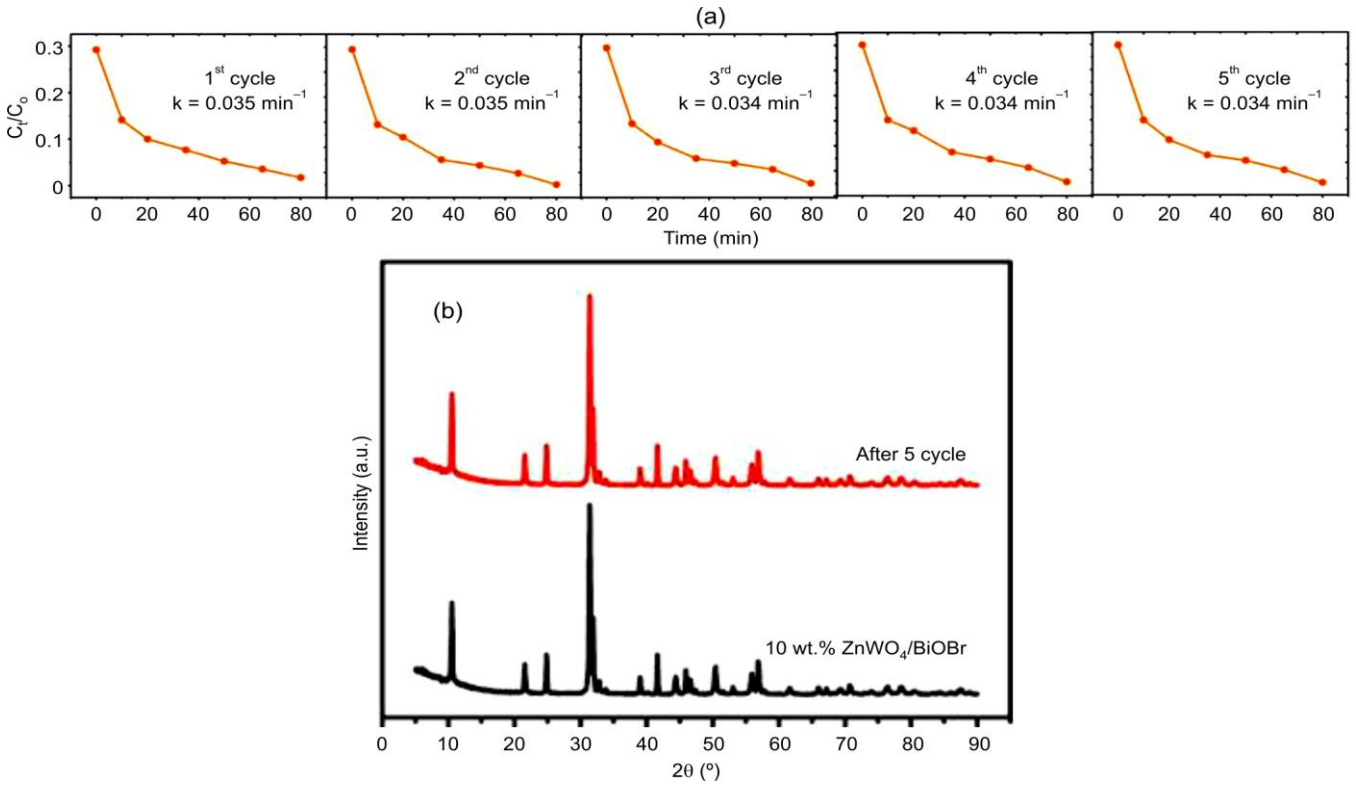

Fig. 6. (a) Reusability assessment and (b) pXRD of pure and used photocatalyst

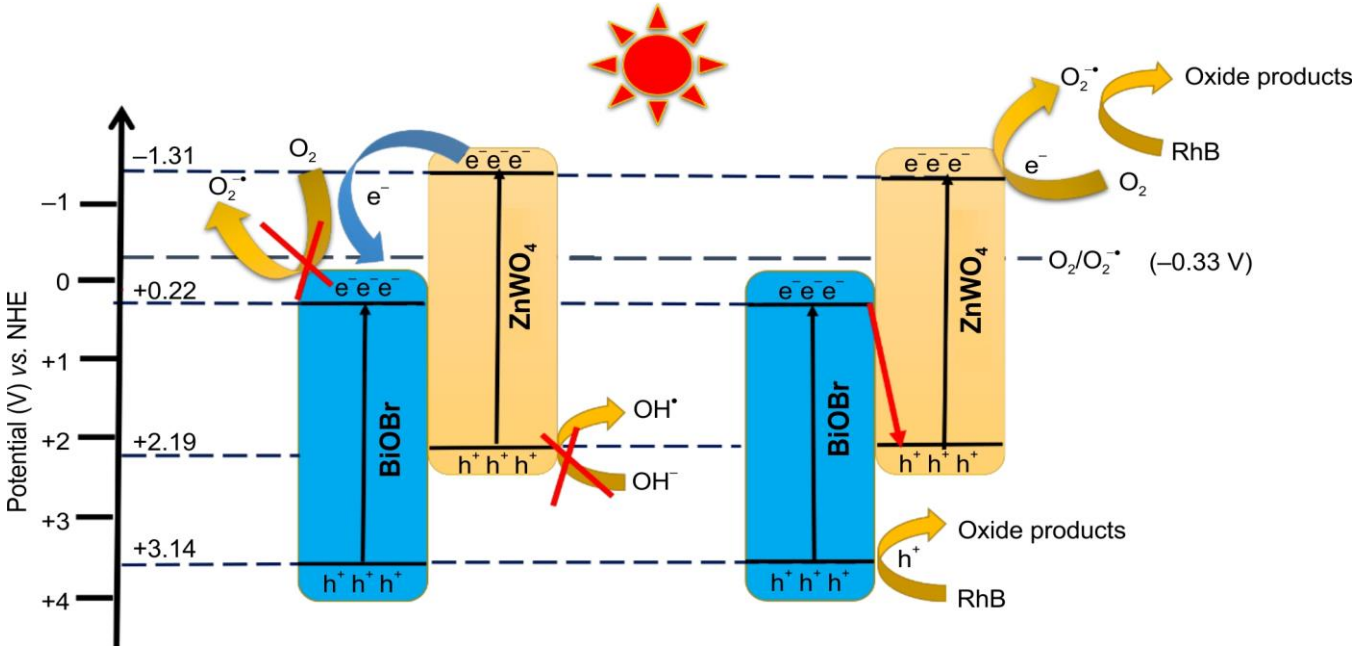

Fig. 7. Potential pathways for the photocatalytic degradation of rhodamine B (RhB) using a $ZnWO_4$/BiOBr nanocomposite

heterojunction. Under sunlight irradiation, both $ZnWO_4$ and BiOBr absorb visible light, leading to the generation of electron-hole pairs. In this configuration, photogenerated electrons in the conduction band of BiOBr, migrate to the valence band of $ZnWO_4$, where they rapidly recombine with photogenerated holes. This charge transfer pathway allows the more reductive electrons in the conduction band of $ZnWO_4$ to remain available, where they can efficiently react with adsorbed oxygen molecules to generate superoxide radicals ($O_2^{-\bullet}$). Simultaneously, the photogenerated holes retained in the valence band of BiOBr can directly oxidize RhB molecules. Furthermore, superoxide radicals may also be generated through a two-electron reduction pathway from hydrogen peroxide or *via* subsequent reactions involving photogenerated holes [29], as described by the following reactions:

$$ZnWO_4 + h\nu \rightarrow e^-_{CB} + h^+_{VB} \quad (1)$$

$$BiOBr + h\nu \rightarrow e^-_{CB} + h^+_{VB} \quad (2)$$

$$BiOBr(e^-_{CB} + h^+_{VB}) + ZnWO_4(e^-_{CB} + h^+_{VB}) \rightarrow BioBr(e^-_{CB}) + ZnWO_4(h^+_{VB}) \quad (3)$$

$$BiOBr(e^-_{CB}) + ZnWO_4(h^+_{VB}) \rightarrow \text{Recombination} \quad (4)$$

$$BiOBr(h^+_{VB}) + RhB_{(aq)} \rightarrow CO_2 + H_2O \quad (5)$$

$$ZnWO_4(e^-_{CB}) + O_2 \rightarrow ZnWO_4 + O_2^{-\bullet} \quad (6)$$

$$O_2^{-\bullet} + RhB_{(aq)} \rightarrow CO_2 + H_2O \quad (7)$$

Conclusion

In this work, $ZnWO_4$/BiOBr heterojunction photocatalyst was successfully synthesized *via in situ* hydrothermal method, demonstrating outstanding photocatalytic performance for the degradation of RhB under natural sunlight irradiation. The 10 wt.% $ZnWO_4$/BiOBr composite exhibited significantly higher photocatalytic efficiency compared to pristine BiOBr, with a degradation rate constant approximately five times greater. This enhanced activity can be attributed to its excellent absorption of visible light and improved charge carrier separation. Moreover, the $ZnWO_4$/BiOBr nanocomposite maintained both its structural integrity and photocatalytic performance over five successive cycles, highlighting its excellent stability and reusability for practical applications.

ACKNOWLEDGEMENTS

The authors are thankful to Prof. R.K Dwivedi (Dean), Teerthanker Mahaveer University, Moradabad, India, for his valuable insight and suggestions for completing this study.

CONFLICT OF INTEREST

The authors declare that there is no conflict of interests regarding the publication of this article.

REFERENCES

1. M.J.F. Calvete, G. Piccirillo, C.S. Vinagreiro and M.M. Pereira, *Coord. Chem. Rev.*, **395**, 63 (2019); https://doi.org/10.1016/j.ccr.2019.05.004
2. R. Daghrir and P. Drogui, *Environ. Chem. Lett.*, **11**, 209 (2013); https://doi.org/10.1007/s10311-013-0404-8
3. J. Fick, H. Söderström, R.H. Lindberg, C. Phan, M. Tysklind and D.G. Larsson, *Environ. Toxicol. Chem.*, **28**, 2522 (2009); https://doi.org/10.1897/09-073.1
4. S. Manzetti and R. Ghisi, *Mar. Pollut. Bull.*, **79**, 7 (2014); https://doi.org/10.1016/j.marpolbul.2014.01.005
5. R. Zhang, J. Tang, J. Li, Z. Cheng, C. Chaemfa, D. Liu, Q. Zheng, M. Song, C. Luo and G. Zhang, *Sci. Total Environ.*, **450–451**, 197 (2013); https://doi.org/10.1016/j.scitotenv.2013.02.024
6. C. Adams, Y. Wang, K. Loftin and M. Meyer, *J. Environ. Eng.*, **128**, 253 (2002); https://doi.org/10.1061/(ASCE)0733-9372(2002)128:3(253)

7. N.A. Khan, S. Ahmed, I.H. Farooqi, I. Ali, V. Vambol, F. Changani, M. Yousefi, S. Vambol, S.U. Khan and A.H. Khan, *Trends Analyt. Chem.*, **129**, 115921 (2020); https://doi.org/10.1016/j.trac.2020.115921
8. Y. Wang, K. Ding, R. Xu, D. Yu, W. Wang, P. Gao and B. Liu, *J. Clean. Prod.*, **247**, 119108 (2020); https://doi.org/10.1016/j.jclepro.2019.119108
9. Y. Wang, D. Yu, W. Wang, P. Gao, S. Zhong, L. Zhang, Q. Zhao and B. Liu, *Sep. Purif. Technol.*, **239**, 116562 (2020); https://doi.org/10.1016/j.seppur.2020.116562
10. R. Yang, Z. Zhu, C. Hu, S. Zhong, L. Zhang, B. Liu and W. Wang, *Chem. Eng. J.*, **390**, 124522 (2020); https://doi.org/10.1016/j.cej.2020.124522
11. L. Zhang, Y. Li, Q. Li, J. Fan, S. A. C. Carabineiro and K. Lv, *Chem. Eng. J.*, **419**, 129484 (2021); https://doi.org/10.1016/j.cej.2021.129484
12. M. Hojamberdiev, K.I. Katsumata, K. Morita, S.A. Bilmes, N. Matsushita and K. Okada, *Appl. Catal. A Gen.*, **457**, 12 (2013); https://doi.org/10.1016/j.apcata.2013.03.014
13. F. Chen, Q. Yang, J. Sun, F. Yao, S. Wang, Y. Wang, X. Wang, X. Li, C. Niu, D. Wang and G. Zeng, *ACS Appl. Mater. Interfaces*, **8**, 32887 (2016); https://doi.org/10.1021/acsami.6b12278
14. G. Zhang, D. Chen, N. Li, Q. Xu, H. Li, J. He and J. Lu, *Appl. Catal. B*, **250**, 313 (2019); https://doi.org/10.1016/j.apcatb.2019.03.055
15. X. Gao, G. Huang, H. Gao, C. Pan, H. Wang, J. Yan, Y. Liu, H. Qiu, N. Ma and J. Gao, *J. Alloys Compd.*, **674**, 98 (2016); https://doi.org/10.1016/j.jallcom.2016.03.031
16. M. Farhan, A.K. Singh and G. Kumar, *Rasayan J. Chem.*, **18**, 913 (2025); https://doi.org/10.31788/RJC.2025.1829245
17. J. Li, H. Yuan, W. Zhang, B. Jin, Q. Feng, J. Huang and Z. Jiao, *Carbon Energy*, **4**, 294 (2022); https://doi.org/10.1002/cey2.179
18. A.P. Chowdhury and B.H. Shambharkar, *Chemical Eng. J. Adv.*, **4**, 100040 (2020); https://doi.org/10.1016/j.ceja.2020.100040
19. Y. Zhang, J. Di, W. Tong, X. Chen, J. Zhao, P. Ding, S. Yin, J. Xia and H. Li, *Res. Chem. Intermed.*, **45**, 437 (2019); https://doi.org/10.1007/s11164-018-3610-y
20. J. Mao, B. Hong, J. Wei, J. Xu, Y. Han, H. Jin, D. Jin, X. Peng, J. Li, Y. Yang, J. Gong, H. Ge and X. Wang, *ChemistrySelect*, **4**, 13716 (2019); https://doi.org/10.1002/slct.201903944
21. Z. Qiang, X. Liu, F. Li, T. Li, M. Zhang, H. Singh, M. Huttula and W. Cao, *Chem. Eng. J.*, **403**, 126327 (2021); https://doi.org/10.1016/j.cej.2020.126327
22. J. Sun, C.H. Shen, J. Guo, H. Guo, Y.F. Yin, X.J. Xu, Z.H. Fei, Z.T. Liu and X.J. Wen, *J. Colloid Interface Sci.*, **588**, 19 (2021); https://doi.org/10.1016/j.jcis.2020.12.043
23. F. Qiu, W. Li, F. Wang, H. Li, X. Liu and J. Sun, *J. Colloid Interface Sci.*, **493**, 1 (2017); https://doi.org/10.1016/j.jcis.2016.12.066
24. J. Hu, X. Li, X. Wang, Q. Li and F. Wang, *Dalton Trans.*, **48**, 8937 (2019); https://doi.org/10.1039/C9DT01184F
25. P. Raizada, P. Thakur, A. Sudhaik, P. Singh, V.K. Thakur and A. Hosseini-Bandegharaei, *Arab. J. Chem.*, **13**, 4538 (2020); https://doi.org/10.1016/j.arabjc.2019.10.001
26. X. Shi, L. Wang, A.A. Zuh, Y. Jia, F. Ding, H. Cheng and Q. Wang, *J. Alloys Compd.*, **903**, 163889 (2022); https://doi.org/10.1016/j.jallcom.2022.163889
27. G. Kumar, *J. Inorg. Organomet. Polym. Mater.*, **33**, 2710 (2023); https://doi.org/10.1007/s10904-023-02711-y
28. W.H. Koppenol, D.M. Stanbury and P.L. Bounds, *Free Radic. Biol. Med.*, **49**, 317 (2010); https://doi.org/10.1016/j.freeradbiomed.2010.04.011
29. M. Kowalkińska, P. Głuchowski, T. Swebocki, T. Ossowski, A. Ostrowski, W. Bednarski, J. Karczewski and A. Zielińska-Jurek, *J. Phys. Chem. C*, **125**, 25497 (2021); https://doi.org/10.1021/acs.jpcc.1c06481